Nuclear polarization in hydrogenlike $^{208}_{82}Pb^{81+}$

Akihiro Haga,[1,*] Yataro Horikawa,[2,†] and Yasutoshi Tanaka[1]
[1]*Department of Environmental Technology and Urban Planning, Nagoya Institute of Technology, Gokiso, Nagoya 466-8555, Japan*
[2]*Department of Physics, Juntendo University, Inba-gun, Chiba 270-1695, Japan*
(Received 4 October 2001; published 8 May 2002)

We calculate nuclear-polarization energy shifts for the hydrogenlike $^{208}_{82}Pb^{81+}$. The retarded transverse part as well as the longitudinal part is taken into account as the electromagnetic interaction between an electron and the nucleus. With a finite charge distribution for the nuclear ground state and the random-phase approximation to describe the nuclear excitations, we obtain nuclear-polarization energy of the $1s_{1/2}$ state as -38.2 (-37.0) meV in the Feynman (Coulomb) gauge. For the $2s_{1/2}$, $2p_{1/2}$, and $2p_{3/2}$ states, they are -6.7 (-6.4), -0.2 (-0.2), and $+0.0$ $(+0.0)$ meV, respectively. The transverse contribution is small in comparison with the longitudinal nuclear-polarization correction. It is about 12% both for the $1s_{1/2}$ and $2s_{1/2}$ states. The seagull term in the two-photon exchange diagrams is also shown to be quite important to obtain the gauge-invariant nuclear-polarization energies.

DOI: 10.1103/PhysRevA.65.052509 PACS number(s): 31.30.Gs, 31.30.Jv, 12.20.Ds

I. INTRODUCTION

High-precision Lamb shift measurement on high-Z hydrogenlike atoms [1] has evoked a renewed interest in the quantum electrodynamic (QED) calculation of electronic atoms. Comparison of theoretical results with corresponding experimental data allows sensitive tests of QED in strong electromagnetic fields [2,3]. Any discrepancy between theory and experiment may either motivate an improvement of theoretical calculations and a refinement of experiments, or it may indicate a possible influence of non-QED effects. In this context, the study of nuclear-polarization (NP) contributions to the total energy shift of atomic levels becomes important because as a background effect, it represents a natural limitation of any high-precision test of QED. Unfortunately, evaluation of NP is not practicable from first principles. Any calculation of NP is inherently phenomenological and depends on the parameters of the nuclear model used to describe the intrinsic nuclear dynamics.

During the past years, a lot of information has been accumulated regarding the calculation of the NP effect for muonic atoms [4]. There it leads to a large correction at a keV level, mainly because of the huge overlap of the muon wave function with a nucleus and because the transition energies in muonic atoms are of the order of magnitude of typical nuclear excitation energies.

Much less attention has been paid to the NP effect for electronic atoms. They turn out to be reduced by orders of magnitude because of the small overlap of the electron wave function with the nucleus and because the transition energies in electronic atoms are, in general, orders of magnitude smaller than typical nuclear excitation energies.

The NP effect for electronic atoms was first calculated in terms of the second-order Schrödinger perturbation theory [5]. A relativistic field-theoretical treatment of the nuclear-polarization calculation was then presented by Plunien and co-workers [6–8] utilizing the concept of effective photon propagators with nuclear-polarization insertions. The formalism allows to take into account the effect of the electron negative-energy intermediate states besides the usual contribution of the electron excited into higher unoccupied intermediate states. They found that in electronic atoms NP energies become small due to the cancellation between contributions of positive-energy states and those of negative-energy states.

In the above studies, only the Coulomb interaction was considered based on the argument that the relative magnitude of transverse interaction is of order of $(v/c)^2$ and the velocity v associated with nuclear dynamics is mainly nonrelativistic. However, the transverse interaction is not negligible in the NP calculation because of the presence of an interference term of order (v/c) between the longitudinal and transverse components of the electromagnetic interaction. In fact the importance of the transverse interaction has been reported for muonic atoms [9,10]. In Ref. [10], the transverse nuclear polarization has been studied in order to explain the discrepancies between theory and experiment in the $2p$ and $3p$ fine-structure splitting energies of muonic $^{208}_{82}Pb$. The contribution for the muonic $1s_{1/2}$ state amounts to 20% of that of the Coulomb interaction.

The transverse interaction could be more important for electronic atoms than for muonic atoms because of its long-range nature. The transverse nuclear polarization for heavy electronic atoms was first studied by Yamanaka and co-workers [11–13] using the Feynman gauge and a collective model for the nuclear excitations. They found that the transverse contribution is several times larger than the Coulomb contribution in heavy electronic atoms before the contributions of the positive- and negative-energy states cancel. However, due to nearly complete cancellation between them, the transverse contribution becomes small and just cancels the Coulomb contribution. As a result, the total NP energy almost vanishes.

The purpose of the present paper is twofold: One is to see how much NP energy is expected for the best model of the

*Electronic address: haga@npl.kyy.nitech.ac.jp
†Electronic address: horikawa@sakura.juntendo.ac.jp

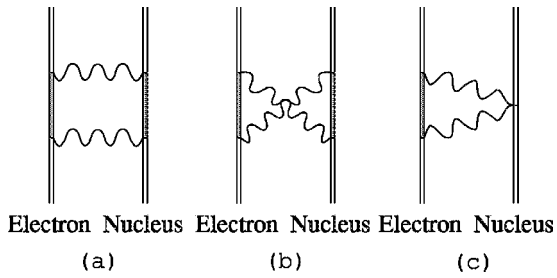

FIG. 1. Diagrams contributing to nuclear polarization in lowest order: (a) ladder, (b) cross, and (c) seagull diagrams.

$^{208}_{82}$Pb nucleus available practically. For this purpose the Dirac-electron wave functions are solved in the Coulomb potential with a finite nuclear charge distribution and the random-phase approximation (RPA) is used to describe the nuclear excitations. The other is to see whether NP energies are sensitive to the choice of the gauge. For this purpose NP energies are calculated in both the Feynman and Coulomb gauges. We will see that the NP calculation with only the ladder and cross diagrams shows large gauge dependence and the inclusion of the seagull diagram removes most of its gauge dependence [14,15].

Calculations are carried out in momentum space. They involve only double integrals, which are easily carried out with high precision.

II. NUCLEAR-POLARIZATION CALCULATION

The second-order contributions to the nuclear polarization are given by three Feynman diagrams in Fig. 1. (Here we regard the seagull graph as one of the nuclear-polarization diagrams.) Two photons are exchanged between a bound electron and a nucleus and the nuclear vertices are understood to have no diagonal matrix elements for the ladder and cross diagrams, and no nuclear intermediate states for the seagull diagram.

The nuclear-polarization energy shift due to the ladder and cross diagrams is given by [6]

$$\Delta E_{NP}=i(4\pi\alpha)^2\int d^4x_1\cdots d^4x_4\overline{\psi}(x_1)\gamma^\mu S_F^e(x_1,x_2)\gamma^\nu \times\psi(x_2)D_{\mu\xi}(x_1,x_3)\Pi_N^{\xi\zeta}(x_3,x_4)D_{\zeta\nu}(x_4,x_2). \quad (1)$$

Here ψ is the electron wave function, S_F^e is the external-field electron propagator, $D_{\mu\xi}$ is the photon propagator, and $\Pi_N^{\xi\zeta}$ is the nuclear-polarization tensor that contains all information about nuclear dynamics. We use units with $\hbar=c=1$ and $e^2=4\pi\alpha$.

In terms of transition charge-current densities, the electron and nuclear parts of Eq. (1) are written as

$$\overline{\psi}(x_1)\gamma^\mu S_F^e(x_1,x_2)\gamma^\nu\psi(x_2) =\int\frac{dE}{2\pi}e^{-iE(t_1-t_2)}\sum_{i'}\frac{j_e^\mu(\boldsymbol{x}_1)_{ii'}j_e^\nu(\boldsymbol{x}_2)_{i'i}}{E-\omega_e+iE_{i'}\epsilon} \quad (2)$$

and

$$\Pi_N^{\xi\zeta}(x_3,x_4)=\int\frac{d\omega}{2\pi}e^{-i\omega(t_3-t_4)}\sum_{I'}\left(\frac{J_N^\xi(\boldsymbol{x}_3)_{II'}J_N^\zeta(\boldsymbol{x}_4)_{I'I}}{\omega-\omega_N+i\epsilon} -\frac{J_N^\zeta(\boldsymbol{x}_4)_{II'}J_N^\xi(\boldsymbol{x}_3)_{I'I}}{\omega+\omega_N-i\epsilon}\right), \quad (3)$$

where $\omega_e=E_{i'}-E_i$ and $\omega_N=E_{I'}-E_I$ are the excitation energies of the electron and the nucleus, respectively. The suffixes $i(I)$ and $i'(I')$ stand for the initial and intermediate states of the electron (nucleus), respectively.

In the momentum representation, NP energy shifts due to the ladder and cross diagrams are written as

$$\Delta E_{NP}^L=-i(4\pi\alpha)^2\int\frac{d\omega}{2\pi}\int\frac{d\boldsymbol{q}}{(2\pi)^3}\int\frac{d\boldsymbol{q}'}{(2\pi)^3}D_{\mu\xi}(\omega,\boldsymbol{q}) \times D_{\zeta\nu}(\omega,\boldsymbol{q}')\sum_{i'}\frac{j_e^\mu(-\boldsymbol{q})_{ii'}j_e^\nu(\boldsymbol{q}')_{i'i}}{\omega+\omega_e-iE_{i'}\epsilon} \times\sum_{I'}\frac{J_N^\xi(\boldsymbol{q})_{II'}J_N^\zeta(-\boldsymbol{q}')_{I'I}}{\omega-\omega_N+i\epsilon} \quad (4)$$

and

$$\Delta E_{NP}^X=i(4\pi\alpha)^2\int\frac{d\omega}{2\pi}\int\frac{d\boldsymbol{q}}{(2\pi)^3}\int\frac{d\boldsymbol{q}'}{(2\pi)^3}D_{\mu\xi}(\omega,\boldsymbol{q}) \times D_{\zeta\nu}(\omega,\boldsymbol{q}')\sum_{i'}\frac{j_e^\mu(-\boldsymbol{q})_{ii'}j_e^\nu(\boldsymbol{q}')_{i'i}}{\omega+\omega_e-iE_{i'}\epsilon} \times\sum_{I'}\frac{J_N^\zeta(-\boldsymbol{q}')_{II'}J_N^\xi(\boldsymbol{q})_{I'I}}{\omega+\omega_N-i\epsilon}, \quad (5)$$

respectively. The substitution

$$\Pi^{\xi\zeta}(x_3,x_4)\rightarrow\frac{\rho_N(\boldsymbol{x}_3)_{II}}{m_p}\delta^{\xi\zeta}\delta^4(x_3-x_4) \quad (6)$$

in Eq. (1) gives the energy correction due to the seagull diagram [14,15],

$$\Delta E_{NP}^{SG}=-i(4\pi\alpha)^2\int\frac{d\omega}{2\pi}\int\frac{d\boldsymbol{q}}{(2\pi)^3}\int\frac{d\boldsymbol{q}'}{(2\pi)^3}D_{\mu\xi}(\omega,\boldsymbol{q}) \times D_{\zeta\nu}(\omega,\boldsymbol{q}')\sum_{i'}\frac{j_e^\mu(-\boldsymbol{q})_{ii'}j_e^\nu(\boldsymbol{q}')_{i'i}}{\omega+\omega_e-iE_{i'}\epsilon} \times\frac{\rho_N(\boldsymbol{q}-\boldsymbol{q}')_{II}}{m_p}\delta^{\xi\zeta}. \quad (7)$$

Here m_p is the proton mass, $\delta^{\xi\zeta}$ is the Kronecker delta extended to four dimensions with $\delta^{00}=0$, and $\rho_N(\boldsymbol{x})_{II}$ is the ground-state charge distribution of the nucleus. The total NP energy shift is given by the sum $\Delta E_{NP}^L+\Delta E_{NP}^X+\Delta E_{NP}^{SG}$.

Substituting the corresponding multipole expansions for the Fourier transform of the currents, these NP energy shifts are written in terms of the multipole form factors defined by

$$\langle i'\|m_\lambda(q)\|i\rangle = \int d\boldsymbol{x}\, j_\lambda(qx)\langle i'\|Y_\lambda(\Omega_x)\rho_e(\boldsymbol{x})\|i\rangle, \quad (8)$$

$$\langle i'\|t_{\lambda L}(q)\|i\rangle = \int d\boldsymbol{x}\, j_L(qx)\langle i'\|\boldsymbol{Y}_{\lambda L}(\Omega_x)\cdot\boldsymbol{j}_e(\boldsymbol{x})\|i\rangle \quad (9)$$

for the electron, and

$$\langle I'\|M_\lambda(q)\|I\rangle = \int d\boldsymbol{x}\, j_\lambda(qx)\langle I'\|Y_\lambda(\Omega_x)\rho_N(\boldsymbol{x})\|I\rangle, \quad (10)$$

$$\langle I'\|T_{\lambda L}(q)\|I\rangle = \int d\boldsymbol{x}\, j_L(qx)\langle I'\|\boldsymbol{Y}_{\lambda L}(\Omega_x)\cdot\boldsymbol{J}_N(\boldsymbol{x})\|I\rangle \quad (11)$$

for the nucleus. In the above equations, $j_\lambda(qx)$ is a spherical Bessel function, $\boldsymbol{Y}_{\lambda L}$ is a vector spherical harmonics, and λ is the multipolarity of transition. With these substitutions, angular parts of $\boldsymbol{q}$ and $\boldsymbol{q}'$ as well as ω integrations in Eqs. (4), (5), and (7) can be carried out analytically. Integrations with respect to q and q' are carried out numerically. Nuclear-polarization energy shifts are thus given by the sum of these double integrals over the nuclear and electron intermediate states. For the seagull contribution, the summation is only over the electron intermediate states.

In the following, we shall give the formula for the NP energy in both the Feynman and Coulomb gauges. We restrict ourselves to $I^\pi = 0^+$ for the spin parity of the nuclear ground state. The spin parity of the nuclear intermediate state I'^π is in this case equal to the spin parity of transition λ^π.

A. The Feynman gauge

The photon propagator in the Feynman gauge is given by

$$D^F_{\mu\xi}(\omega,\boldsymbol{q}) = -\frac{g_{\mu\xi}}{q^2+i\epsilon}. \quad (12)$$

Here the metric tensor $g_{\mu\xi}$ is defined by $g_{00}=1$ and $g_{ii}=-1$. With this propagator, the NP energies due to the ladder, cross, and seagull terms are given by

$$\Delta E^L_{NP} = -\sum_{i'I'} \frac{(4\pi\alpha)^2}{(2i+1)(2I'+1)}\left(\frac{2}{\pi}\right)^2 \int_0^\infty dq \int_0^\infty dq' \times I_+(q,q')\mathcal{W}^F_L(q)\mathcal{W}^F_L(q'), \quad (13)$$

$$\Delta E^X_{NP} = -\sum_{i'I'} \frac{(4\pi\alpha)^2}{(2i+1)(2I'+1)}\left(\frac{2}{\pi}\right)^2 \int_0^\infty dq \int_0^\infty dq' \times I_-(q,q')\mathcal{W}^F_X(q)\mathcal{W}^F_X(q'), \quad (14)$$

$$\Delta E^{SG}_{NP} = -\sum_{i'} \frac{(4\pi\alpha)^2}{(2i+1)}\left(\frac{2}{\pi}\right)^2 \int_0^\infty dq \int_0^\infty dq' I_{SG}(q,q') \times \mathcal{W}^F_{SG}(q,q'). \quad (15)$$

The q and q' integrals may be improper in case of the NP calculation for the electron excited states. In such cases, we should evaluate them by

$$\int \frac{dq}{q\pm i\epsilon} = \mathrm{P}\frac{1}{q} \mp i\pi\delta(q), \quad (16)$$

where P denotes the Cauchy principal value. The second term on the right-hand side of Eq. (16) means that the energy shift is, in general, complex valued. While the real part describes the physical energy shift of the bound state, the imaginary part gives the decay rate of the bound state due to possible transitions of the electron into lower-lying unoccupied bound states.

In the above expressions, I_+, I_-, and I_{SG} are functions written as

$$I_\pm(q,q') = \frac{qq'}{2(\tilde{\omega}_e+q)(\tilde{\omega}_e+q')(\omega_N+q)(\omega_N+q')} \times\left\{ \mathrm{sgn}(E_{i'})\left[\frac{\tilde{\omega}_e\omega_N}{q+q'} + (\tilde{\omega}_e+\omega_N+q+q')\right] \pm\frac{qq'}{q+q'} \pm \theta(\pm E_{i'})\frac{2qq'}{\omega_N+\tilde{\omega}_e}\right\}, \quad (17)$$

$$I_{SG}(q,q') = \mathrm{sgn}(E_{i'})\frac{1}{2m_p}\frac{qq'(\tilde{\omega}_e+q+q')}{(q+q')(q+\tilde{\omega}_e)(q'+\tilde{\omega}_e)}, \quad (18)$$

where $\tilde{\omega}_e = \mathrm{sgn}(E_{i'})\omega_e$, while $\mathcal{W}^F_L(q)$, $\mathcal{W}^F_X(q)$, and $\mathcal{W}^F_{SG}(q)$ are written in terms of the electron and nuclear form factors as

$$\mathcal{W}^F_L(q) = \sum_\lambda \left[\langle i'\|m_\lambda(q)\|i\rangle\langle I'\|M_\lambda(q)\|I\rangle - \sum_{L=\lambda-1}^{\lambda+1} \times(-1)^{L+1-\lambda}\langle i'\|t_{\lambda L}(q)\|i\rangle\langle I'\|T_{\lambda L}(q)\|I\rangle\right], \quad (19)$$

$$\mathcal{W}^F_X(q) = \sum_\lambda \left[\langle i'\|m_\lambda(q)\|i\rangle\langle I'\|M_\lambda(q)\|I\rangle + \sum_{L=\lambda-1}^{\lambda+1}\langle i'\|t_{\lambda L}(q)\|i\rangle\langle I'\|T_{\lambda L}(q)\|I\rangle\right], \quad (20)$$

$$\mathcal{W}^F_{SG}(q,q') = \sum_\lambda \sum_{L=\lambda-1}^{\lambda+1}\langle i'\|t_{\lambda L}(q)\|i\rangle\langle I\|M_L(q,q')\|I\rangle \times\langle i'\|t_{\lambda L}(q')\|i\rangle. \quad (21)$$

The seagull term contains the Fourier transform of the nuclear ground state,

$$\langle I\|M_L(q,q')\|I\rangle=\int r^2dr\rho_N(r)_{II}j_L(qr)j_L(q'r). \quad (22)$$

B. The Coulomb gauge

The photon propagator in the Coulomb gauge is given by

$$D^C_{00}(\omega,\boldsymbol{q})=\frac{1}{q^2+i\epsilon},\quad D^C_{ij}(\omega,\boldsymbol{q})=\frac{1}{q^2+i\epsilon}\left(\delta_{ij}-\frac{q_iq_j}{|\boldsymbol{q}|^2}\right), \quad (23)$$

and $(\delta_{ij}-q_iq_j/|\boldsymbol{q}|^2)$ in D^C_{ij} projects out both transverse parts of electronic and nuclear currents.

Making use of the relation

$$\boldsymbol{j}^T_e(-\boldsymbol{q})\cdot\boldsymbol{J}^T_N(\boldsymbol{q})=\boldsymbol{j}_e(-\boldsymbol{q})\cdot\boldsymbol{J}_N(\boldsymbol{q})+\frac{\omega_e\omega_N}{q^2}\rho_e(-\boldsymbol{q})\rho_N(\boldsymbol{q}), \quad (24)$$

we obtain NP energies for the ladder, cross, and seagull terms as

$$\Delta E^L_{NP}=-\sum_{i'I'}\frac{(4\pi\alpha)^2}{(2i+1)(2I'+1)}\int_0^\infty dq\int_0^\infty dq' \times\left\{\frac{\theta(E_{i'})}{\tilde{\omega}_e+\omega_N}\mathcal{W}^C_L(q)\mathcal{W}^C_L(q')+I_+(q,q') \times\mathcal{W}^C_T(q)\mathcal{W}^C_T(q')+I^{LT}_+(q')\mathcal{W}^C_L(q)\mathcal{W}^C_T(q')\right\}, \quad (25)$$

$$\Delta E^X_{NP}=-\sum_{i'I'}\frac{(4\pi\alpha)^2}{(2i+1)(2I'+1)}\int_0^\infty dq\int_0^\infty dq' \times\left\{\frac{-\theta(-E_{i'})}{\tilde{\omega}_e+\omega_N}\mathcal{W}^C_L(q)\mathcal{W}^C_L(q')+I_-(q,q') \times\mathcal{W}^C_T(q)\mathcal{W}^C_T(q')+I^{LT}_-(q')\mathcal{W}^C_L(q)\mathcal{W}^C_T(q')\right\}, \quad (26)$$

$$\Delta E^{SG}_{NP}=-\sum_{i'}\frac{(4\pi\alpha)^2}{(2i+1)}\left(\frac{2}{\pi}\right)^2\int_0^\infty dq\int_0^\infty dq' I_{SG}(q,q') \times\mathcal{W}^C_{SG}(q,q'). \quad (27)$$

In the above expressions, $I^{LT}_+(q')$ and $I^{LT}_-(q')$ come from the interference between the longitudinal and transverse terms and are given by

$$I^{LT}_\pm(q')=\pm\frac{\mathrm{sgn}(E_{i'})q'(\tilde{\omega}_e+\omega_N)\pm\theta(\pm E_{i'})2q'^2}{(q'+\tilde{\omega}_e)(q'+\omega_N)(\tilde{\omega}_e+\omega_N)}. \quad (28)$$

In the Coulomb gauge, $\mathcal{W}^C_L(q)$, $\mathcal{W}^C_L(q)$, and $\mathcal{W}^C_L(q)$ are given by

$$\mathcal{W}^C_L(q)=\sum_\lambda\langle i'\|m_\lambda(q)\|i\rangle\langle I'\|M_\lambda(q)\|I\rangle, \quad (29)$$

$$\mathcal{W}^C_T(q)=-\sum_\lambda\left[\frac{\omega_e\omega_N}{q^2}\mathcal{W}^C_L(q)+\sum_{L=\lambda-1}^{\lambda+1}\langle i'\|t_{\lambda L}(q)\|i\rangle \times\langle I'\|T_{\lambda L}(q)\|I\rangle\right], \quad (30)$$

$$\mathcal{W}^C_{SG}(q,q')=\sum_\lambda\left[\sum_{L=\lambda\pm1}[\langle i'\|u_{\lambda L}(q)\|i\rangle\langle I\|M_L(q,q')\|I\rangle \times\langle i'\|u_{\lambda L}(q')\|i\rangle]+\langle i'\|t_{\lambda\lambda}(q)\|i\rangle \times\langle I\|M_\lambda(q,q')\|I\rangle\langle i'\|t_{\lambda\lambda}(q')\|i\rangle\right] \quad (31)$$

with

$$\langle i'\|u_{\lambda\lambda-1}(q)\|i\rangle=\langle i'\|t_{\lambda-1}(q)\|i\rangle -i\sqrt{\frac{\lambda}{2\lambda+1}}\frac{\omega_e}{q}\langle i'\|m_\lambda(q)\|i\rangle, \quad (32)$$

$$\langle i'\|u_{\lambda\lambda+1}(q)\|i\rangle=\langle i'\|t_{\lambda+1}(q)\|i\rangle -i\sqrt{\frac{\lambda+1}{2\lambda+1}}\frac{\omega_e}{q}\langle i'\|m_\lambda(q)\|i\rangle. \quad (33)$$

C. Electron-wave functions

The radial Dirac equations for the electron are written as

$$\left(\frac{d}{dr}+\frac{\kappa}{r}\right)G_{E,\kappa}=[m_e+E-V(r)]F_{E,\kappa}(r), \quad (34)$$

$$\left(\frac{d}{dr}-\frac{\kappa}{r}\right)F_{E,\kappa}=[m_e-E+V(r)]G_{E,\kappa}(r), \quad (35)$$

where the potential $V(r)$ is obtained from the the ground-state charge distribution of ^{208}Pb, which is assumed to be a two-parameter Fermi distribution

$$\rho_N(r)_{II}=\frac{\rho_0}{1+\exp[(r-R_0)/a]} \quad (36)$$

with $R_0=6.6477$ fm and $a=0.5234$ fm [10]. These equations are solved numerically by using the fourth-order Runge-Kutta method. Both for the positive- and negative-energy continuum states, the radial functions are normalized as

$$G_{E,\kappa}\underset{r\to\infty}{\to}\left(\frac{|E+m_e|}{\pi p}\right)^{1/2}\sin(pr+\delta), \quad (37)$$

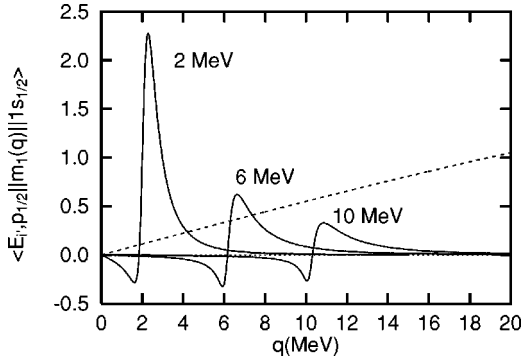

FIG. 2. Electronic Coulomb form factors $\langle E_{i'}, p_{1/2}\|m_1(q)\|1s_{1/2}\rangle$ for the $E_{i'}=2$-, 6-, and 10-MeV states (solid line). The dotted line is the nuclear Coulomb form factor for the 14.6-MeV 1^- state.

$$F_{E,\kappa} \underset{r\to\infty}{\to} \left(\frac{|E-m_e|}{\pi p}\right)^{1/2} \cos(pr+\delta) \tag{38}$$

with $p=\sqrt{E^2-m_e^2}$. Bound-state wave functions are normalized as $\int_0^\infty (G_{n\kappa}^2+F_{n\kappa}^2)dr=1$.

Transition form factors for the electron, Eqs. (8) and (9), are calculated by using the formula given in Ref. [10]. They are stored in the computer with six different step sizes of Δq depending on the electron energy $E_{i'}$. In Fig. 2, we show $E1$ charge form factors $\langle E_{i'}, p_{1/2}\|m_1(q)\|1s_{1/2}\rangle$ of the electron with three different energies, $E_{i'}=2$, 6, and 10 MeV. One finds that they have sharp peaks at $q=E_{i'}$ and decrease rapidly as q increases. Numerical integrations in Eqs. (13)–(15) and (25)–(27) are performed by Simpson's one-third rule.

Most of the NP correction come from the continuum states with energies greater than m_e and less than $-m_e$. Summation over the electron states i' in Eqs. (13)–(15) and Eqs. (25)–(27) implies integration with respect to $E_{i'}$. Integration with respect to $E_{i'}$ is carried out by using the Gauss-Legendre quadrature over the intervals -250 MeV$<E_{i'}<-m_e$ and $m_e<E_{i'}<250$ MeV. Accuracy of numerical results is checked by comparing them with those of Simpson's rule. We also included the electron bound states for $n'\leqslant 7$ in the calculation.

D. RPA calculation of nuclear charge and current densities

The random-phase approximation is used to describe the nuclear excitations. The RPA theory is the most successful microscopic theory to calculate the excitation spectrum of ^{208}Pb. Our RPA spectrum of ^{208}Pb agrees very well with a number of experimental measurements as well as with the most dependable sum rules, which is crucial to estimate the correct magnitude of the NP correction. The model was also applied with success to the NP calculation of muonic ^{208}Pb [10,16]. We thus have confidence that our results are considerably more reliable than the earlier calculations.

The RPA calculation we employed is the same as those performed earlier in Ref. [10], i.e., the same single-particle basis, the same particle-hole configuration of approximately a full $3\hbar\omega$ space, and the same Migdal force [17] parameters to describe nuclear two-body interaction. Nuclear transition form factors, Eqs. (10) and (11), are calculated by assuming the impulse charge-current operators.

TABLE I. The energy-weighted sums of $B(E\lambda)$ over the RPA states. The classical EWSR values [18] are also shown for comparison. The values are given in units of $e^2\,b^\lambda$ MeV.

$E\lambda$	Present calculation	Classical EWSR[a]
$E0$[b]	1.97	1.64
$E1$[c]	8.15	7.38
$E2$	22.2	20.5
$E3$	24.4	23.4
$E4$	14.2	23.6
$E5$	11.3	23.1
$M1$[d]	294	

[a]The radial moments $\langle r^\lambda\rangle_p$ in the classical EWSR are calculated by the Fermi charge distribution (36).
[b]The $E0$ operator is defined as $O(E0)=\Sigma_p r^2/\sqrt{4\pi}$.
[c]The $E1$ operator is defined as $O(E1)=\Sigma_i -1/2\tau_3 r Y_{1\mu}$.
[d]The value given in units of μ_N MeV.

The calculated charge and magnetic-current densities are examined by comparing with experimental $B(E\lambda)$ and $B(M\lambda)$ using the relations

$$B(E\lambda: I\to I') = \frac{1}{2I+1}\left| e\int \rho_{N\lambda}^{I'I}(r) r^{\lambda+2} dr\right|^2 \tag{39}$$

and

$$B(M\lambda: I\to I') = \frac{1}{2I+1}\frac{\lambda}{\lambda+1}\left| e\int J_{N\lambda\lambda}^{I'I}(r) r^{\lambda+2} dr\right|^2. \tag{40}$$

In Table I, we compared the energy-weighted sum of $B(E\lambda)$ over the RPA states with the classical energy-weighted sum-rule value (EWSR) of Ref. [18]. The results for the $E0$ and $E1$ transitions exceed the EWSR by 20% and 10%, respectively, while the results for the $E2$ and $E3$ transitions agree well with the EWSR. For the $E4$ and $E5$ transitions, our results exhaust only 50% of the EWSR. This may be due to the insufficient configuration space for the $E4$ and $E5$ calculations.

On the other hand, there is no experimental constraint imposed on the nuclear electric current. However, the electromagnetic current should satisfy the continuity equation required by charge conservation,

$$\frac{\partial}{\partial t}\rho_N + \boldsymbol{\nabla}\cdot\boldsymbol{J}_N = 0. \tag{41}$$

Using the nuclear Hamiltonian H_N, we rewrite it as

$$i[H_N, \rho_N] + \boldsymbol{\nabla}\cdot\boldsymbol{J}_N = 0. \tag{42}$$

Taking the matrix element of Eq. (42) between the initial and the final nuclear states, we obtain the charge conservation condition

$$i\omega_N \rho_{N\lambda}^{I'I}(r) = -\sqrt{\frac{\lambda}{2\lambda+1}}\left(\frac{d}{dr} - \frac{\lambda-1}{r}\right) J_{N\lambda\lambda-1}^{I'I}(r) + \sqrt{\frac{\lambda+1}{2\lambda+1}}\left(\frac{d}{dr} + \frac{\lambda+2}{r}\right) J_{N\lambda\lambda+1}^{I'I}(r). \tag{43}$$

Here, $\omega_N = E_{I'} - E_I$ is the energy of nuclear excitation.

For any kind of model calculation involving the nuclear current, it is necessary for the model to satisfy the charge conservation condition in order to observe the gauge invariance [14]. Unfortunately, the charge-current densities constructed from the present RPA calculation do not satisfy the charge conservation of Eq. (43). The violation of charge conservation comes from the inconsistency of using empirical single-particle energies together with the impulse charge-current operators, as is discussed in Refs. [10,19]. It is desirable if one could construct a microscopic self-consistent model together with the nuclear current satisfying the charge conservation, which is realistic enough to reproduce the observed spectra and $B(E\lambda)$ values. However, the refinement of the calculation will be left for the future and at present we are satisfied with the fact that the calculated NP energies show only a small gauge violation even though empirical single-particle energies are used in the RPA calculation.

III. RESULTS AND DISCUSSION

Nuclear-polarization energy shifts are obtained by computing an energy shift for each of the RPA excitations and summing the results. Our calculation gives 38, 129, 160, 222, 202, 218, and 70 nuclear states for the 0^+, 1^-, 2^+, 3^-, 4^+, 5^-, and 1^+ excitations, respectively. Figure 3 shows the NP energy spectra of the $1s_{1/2}$ state for the respective nuclear spins and parities. These spectra are calculated in the Coulomb gauge with the Coulomb and transverse parts of the electromagnetic interaction. They are very similar to the RPA spectra of $B(E\lambda)$ and $B(M1)$.

Table II summarizes the NP energies of the $1s_{1/2}$ state for $^{208}_{82}\mathrm{Pb}^{81+}$. The first column denotes nuclear spins and parities. The entries in the second column indicate the contributions to the NP energy from the ladder, cross, and seagull terms as well as those of the positive- and negative-energy intermediate states of the electron. The third column shows the NP energies in the Feynman gauge, while the fourth column shows the NP energies in the Coulomb gauge. The transverse contributions are included in both columns. The fifth column shows the Coulomb NP energies without the transverse contribution (hereafter referred to as CNP). The sixth column shows the results of the previous NP calculation in the Feynman gauge assuming a collective model for the nuclear excitations [13]. The seventh column is the CNP from the same model. Finally, the last column shows the CNP calculated in Ref. [8].

First of all, the present CNP energies is compared with the previous calculations. They are -33.2 meV (fifth column), -35.5 meV (seventh column), and -29.3 meV (eighth column). The present calculation employs RPA charge densities, while the previous ones are based on the collective-model charge densities. They agree fairly well. The 10% variation between the fifth and eighth columns may be attributed to the energy-weighted sum of $B(E\lambda)$ over the RPA states, which exceeds the classical EWSR value by 20% for the $E0$ transition and 10% for the $E1$ transition. On the other hand, there exists 20% variation between the seventh and eighth columns, though they are based on the same collective model. The difference is conspicuous only for the monopole NP energy, i.e., -7.2 meV (seventh column) and -3.3 meV (eighth column). The difference may be attributed to the Dirac-electron wave functions used; those for the finite charge distribution are used in the eighth column, while those for the point charge are used in the seventh column. The electron wave functions generated from the point charge and the finite charge distribution differ appreciably only inside the nucleus and that is exactly the region where the monopole nuclear potential exists.

In Table II, we see that the nuclear dipole states give predominant NP contribution. The table also reveals that surprisingly large cancellations occur in the resulting NP energy. The ladder, cross, and seagull diagrams in Fig. 1 all give large contributions to the NP energy if their contributions from the positive- and negative-energy electron states are separately considered. The positive- and negative-energy electron states contribute to the NP energy with opposite signs in each of the diagrams, the fact that is also observed in Refs. [8,13]. Besides, the positive- and negative-energy states in the seagull term contribute to the NP energy with signs opposite to those of the ladder and cross terms. Neglecting any one of these can introduce a nonnegligible change in the NP energy, while inclusion of all these produces a very small result, because of the cancellation. The total $E1$ NP energy differs from the CNP energy by 30%.

The dominance of the $E1$ contribution to the NP energy can be seen clearly in the spectral NP density of a nuclear excitation as a function of electron energy. In Fig. 4, spectral densities in the Coulomb gauge are shown for three different nuclear states: (a) 0^+ (13.3 MeV), (b) 1^- (14.6 MeV), and (c) 2^+ (10.2 MeV). In each panel, the solid line shows the spectral density including the transverse contribution, while the dotted line shows the result without the transverse effect. One can see that the low-energy region of the 1^- state [Fig. 4(b)] is different from the other two. The 1^- spectrum shows the peak at threshold ($E_{i'} = m_e$). The peak is produced by the nonvanishing matrix elements of $\langle I' \| T_{10}(q) \| I \rangle$ and $\langle i' \| t_{10}(q) \| i \rangle$ at $q = 0$.

An important feature of the present calculation, which is in fact crucial for the numerical estimate of NP energies, is that there exists a large violation of gauge invariance in the NP energy shifts as far as only the ladder and cross diagrams of Figs. 1(a) and 1(b) are taken into account. By using the minimal prescription, the nonrelativistic electromagnetic interaction involves the square of vector potential called a seagull term coming from the kinetic energy, and this term is necessary for the gauge invariance in a nonrelativistic system

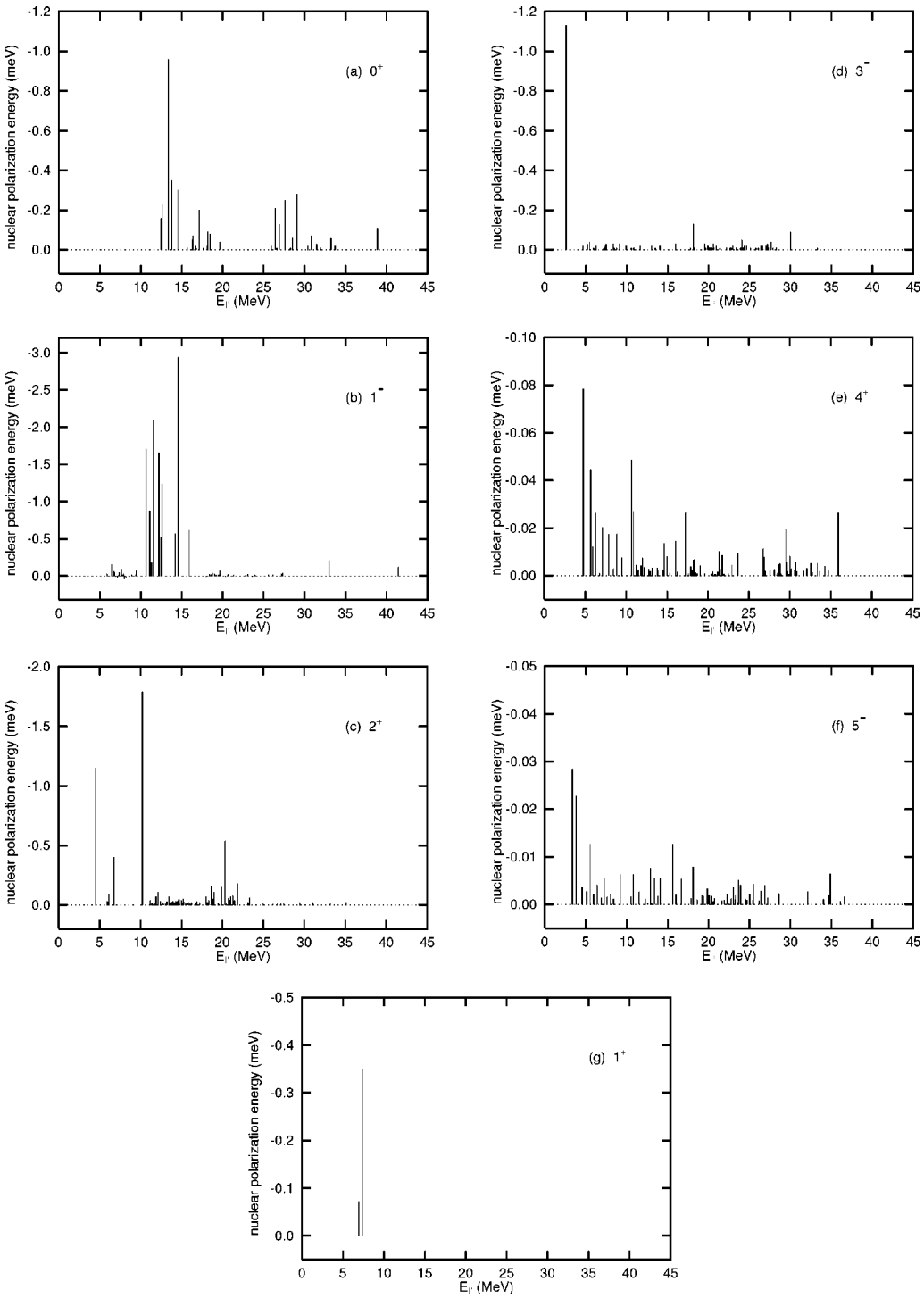

FIG. 3. Nuclear-polarization spectra as a function of nuclear excitation energy. The Coulomb gauge is assumed.

[14,15]. It is interesting to investigate whether the inclusion of the seagull term restores the gauge invariance of the present NP calculation. (A proof of the gauge invariance is given in the Appendix.)

As seen from Table II, this is nicely confirmed numerically. With the ladder and cross diagrams, the NP energy for the $1s_{1/2}$ was $+1.5$ meV in the Feynman gauge, while being -32.7 meV in the Coulomb gauge. The gauge dependence was 34.2 meV. However, after the inclusion of the seagull term, it is -38.2 meV in the Feynman gauge and -37.0 meV in the Coulomb gauge. The gauge dependence is reduced to 1.2 meV. This small gauge dependence shows that the seagull term is quite important in restoring the gauge invariance of the NP calculation. The fact also implies that the use of empirical single-particle energies in the RPA calculation does not introduce a serious violation of gauge invariance into the NP energies.

For the excited L-shell electrons, we can repeat the dis-

TABLE II. Nuclear-polarization correction (meV) to the $1s_{1/2}$ state of $^{208}_{82}Pb^{81+}$. Energy shifts ΔE^L, ΔE^X, and ΔE^{SG} are contributions of the ladder, cross, and seagull terms, respectively, while ΔE^+ (ΔE^-) denotes contribution from the positive- (negative-) energy intermediate states of the electron.

λ^π	Contribution	Present[a] Feynman NP	Present[b] Coulomb NP	Present[c] CNP	Ref. [13][d] NP	Ref. [13][e] CNP	Ref. [8][f] CNP
0^+	ΔE^{L+}	−5.7	−6.5	−7.0			
	ΔE^{L-}	+0.4	+0.2				
	ΔE^{X+}	−1.2	−0.2				
	ΔE^{X-}	+2.7	+2.7	+3.0			
	$\Delta E^L+\Delta E^X$	−3.8	−3.9	−4.0	−6.6	−7.2	−3.3
	ΔE^{SG+}	+0.7	0.0				
	ΔE^{SG-}	−0.9	0.0				
	$\Delta E^L+\Delta E^X+\Delta E^{SG}$	−3.9	−3.9				
1^-	ΔE^{L+}	−119.1	−91.1	−37.0			
	ΔE^{L-}	+74.0	+37.6				
	ΔE^{X+}	−49.8	−29.4				
	ΔE^{X-}	+110.1	+64.2	+16.7			
	$\Delta E^L+\Delta E^X$	+15.2	−18.7	−20.3	+16.3	−19.5	−17.6
	ΔE^{SG+}	+144.2	+87.8				
	ΔE^{SG-}	−186.5	−95.1				
	$\Delta E^L+\Delta E^X+\Delta E^{SG}$	−27.1	−26.0				
2^+	ΔE^{L+}	−13.0	−15.3	−14.4			
	ΔE^{L-}	+2.0	+0.4				
	ΔE^{X+}	−3.2	−0.5				
	ΔE^{X-}	+8.1	+9.1	+8.6			
	$\Delta E^L+\Delta E^X$	−6.1	−6.3	−5.8	−7.0	−6.3	−5.8
	ΔE^{SG+}	+4.4	+2.7				
	ΔE^{SG-}	−4.1	−2.1				
	$\Delta E^L+\Delta E^X+\Delta E^{SG}$	−5.7	−5.7				
3^-	ΔE^{L+}	−5.0	−6.5	−6.3			
	ΔE^{L-}	+1.0	+0.1				
	ΔE^{X+}	−1.6	−0.1				
	ΔE^{X-}	+3.2	+4.1	+4.0			
	$\Delta E^L+\Delta E^X$	−2.4	−2.4	−2.3	−2.9	−2.6	−2.6
	ΔE^{SG+}	+1.0	+0.6				
	ΔE^{SG-}	−0.8	−0.4				
	$\Delta E^L+\Delta E^X+\Delta E^{SG}$	−2.2	−2.2				
4^+	ΔE^{L+}	−1.1	−1.5	−1.4			
	ΔE^{L-}	+0.2	0.0				
	ΔE^{X+}	−0.4	0.0				
	ΔE^{X-}	+0.7	+0.8	+0.8			
	$\Delta E^L+\Delta E^X$	−0.7	−0.7	−0.6			
	ΔE^{SG+}	+0.5	+0.4				
	ΔE^{SG-}	−0.4	−0.3				
	$\Delta E^L+\Delta E^X+\Delta E^{SG}$	−0.6	−0.6				
5^-	ΔE^{L+}	−0.4	−0.5	−0.4			
	ΔE^{L-}	+0.1	0.0				
	ΔE^{X+}	−0.1	0.0				
	ΔE^{X-}	+0.2	+0.2	+0.2			
	$\Delta E^L+\Delta E^X$	−0.2	−0.2	−0.2			

TABLE II. (*Continued*).

λ^{π}	Contribution	Present[a] Feynman NP	Present[b] Coulomb NP	Present[c] CNP	Ref. [13][d] NP	Ref. [13][e] CNP	Ref. [8][f] CNP
	ΔE^{SG+}	+0.3	+0.1				
	ΔE^{SG-}	−0.2	−0.1				
	$\Delta E^{L}+\Delta E^{X}+\Delta E^{SG}$	−0.2	−0.2				
1^{+}	ΔE^{L+}	−0.4	−0.4				
	ΔE^{L-}	+0.1	+0.1				
	ΔE^{X+}	−0.2	−0.2				
	ΔE^{X-}	+0.1	+0.1				
	$\Delta E^{L}+\Delta E^{X}$	−0.4	−0.4				
	ΔE^{SG+}	+3.8	+3.8				
	ΔE^{SG-}	−1.7	−1.7				
	$\Delta E^{L}+\Delta E^{X}+\Delta E^{SG}$	+1.7	+1.7				
Total							
	ΔE^{L+}	−144.7	−121.8	−66.5			
	ΔE^{L-}	+77.8	+38.3				
	ΔE^{X+}	−56.7	−30.4				
	ΔE^{X-}	+125.1	+81.2	+33.3			
	$\Delta E^{L}+\Delta E^{X}$	+1.5	−32.7	−33.2	−0.2	−35.5	−29.3
	ΔE^{SG+}	+154.9	+95.4				
	ΔE^{SG-}	−194.6	−99.7				
	$\Delta E^{L}+\Delta E^{X}+\Delta E^{SG}$	−38.2	−37.0				

[a]The NP energies in the Feynman gauge.
[b]The NP energies in the Coulomb gauge.
[c]The unretarded NP energies in the Coulomb gauge.
[d]The NP energies evaluated in the Feynman gauge. Electron wave functions were solved by assuming the point charge for the nuclear ground state. Nuclear transition charge densities were determined by a collective model. They were normalized to the observed $B(E\lambda)$ for the low-lying nuclear states and EWSR values for the high-lying giant resonances. Nuclear current densities $J_{N\lambda\lambda-1}(r)$ were obtained by solving the equation of charge conservation (43) assuming $J_{N\lambda\lambda+1}(r)=0$.
[e]Same as footnote d except for the unretarded NP energies.
[f]The unretarded NP energies. Same as footnote e except for the electron wave functions solved by assuming a finite charge distribution for the nuclear ground state.

cussion that the $E1$ multipole plays a main role in the NP effects of hydrogenlike atoms and essentially determines the magnitude of the NP energy.

The total NP energies for the $1s_{1/2}$, $2s_{1/2}$, $2p_{1/2}$, and $2p_{3/2}$ states are summarized in Table III and are compared with the CNP energies of the present calculation and those of Ref. [8]. The transverse contribution is small in comparison with the CNP contribution. It is about 12% both for the $1s_{1/2}$ and $2s_{1/2}$ states. In spite of large cancellation involved in the calculation, the resulting NP energies become very close to the CNP energies. The present results may indicate that the gauge-invariant contributions of the order of (v/c) and $(v/c)^2$ are small in comparison with the contribution of the order of $(v/c)^0$. The results confirm the estimates for the NP corrections of Ref. [8]. They indicate that within the collective-model approach, the gauge-invariant contribution up to order $(v/c)^0$ can be deduced from the longitudinal part of the effective photon propagator only when the Coulomb gauge is employed. A relatively large transverse contribution is seen in the NP energy of the $2p_{1/2}$ state, though the NP energy of this state is negligibly small. This is due to the $E1$ transition from the $2p_{1/2}$ state to the lower-lying $1s_{1/2}$ state. The transverse component is dominant in the transition as seen from the peak in the 1^- spectrum of Fig. 4(b).

Since the nuclear dipole states have predominant NP contributions, we must note here effects of the spurious center-of-mass motion of the nucleus on the NP energies. The present Migdal force brings down the lowest 1^- state to the imaginary eigenvalue of $1.32i$ MeV. Since this 1^- state carries most of the spurious center-of-mass motion, we excluded this nuclear state from the NP calculation. The 0.7% of the spurious center-of-mass motion remains in the rest of the 1^- states, whose effects on the NP energies are negligible. Thus our results for NP energy due to the cross and ladder diagrams contain intrinsic excitations only. On the other hand, the seagull contributions calculated by using Eq. (22) contain effects of both intrinsic excitations and the center-of-mass motion. The seagull contribution coming from the center-of-mass motion must be eliminated for the dipole mode. This was achieved by using the effective dipole

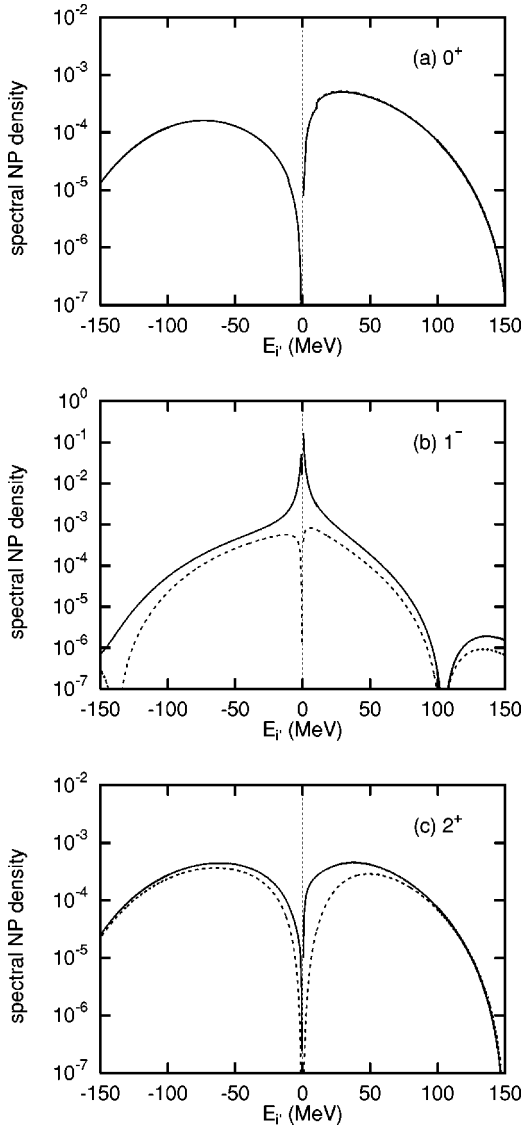

FIG. 4. Spectral NP densities with no dimensions for (a) 0^+ 13.3-MeV, (b) 1^- 14.6-MeV, and (c) 2^+ 10.2-MeV states as a function of electron energy $E_{i'}$. Nuclear-polarization energy is given by the integral of spectral density over $E_{i'}$. The solid line denotes the calculation with both the Coulomb and transverse parts of the electromagnetic interaction, while the dotted line denotes the calculation with only the Coulomb part of the interaction. Electron intermediate states (a) $|E_{i'},s_{1/2}\rangle$, (b) $|E_{i'},p_{1/2}\rangle$, and (c) $|E_{i'},d_{3/2}\rangle$ are assumed in the respective panels.

charges $e_p=N/A$, $e_n=-Z/A$ instead of using the true charges $e_p=1$, $e_n=0$.

IV. SUMMARY

We have calculated the NP energy shifts for the hydrogenlike $^{208}_{82}Pb^{81+}$ taking into account the effects of the electron in the negative-energy continuum, in addition to the usual contributions of the electron excited into higher unoccupied orbitals. Evaluation of NP energy contains the seagull graph as well as the ladder and cross diagrams. The Dirac-electron wave functions were solved in the Coulomb potential with a finite charge distribution for the nuclear ground state and the RPA wave functions were employed for the nuclear excited states. The impulse charge-current operators were assumed in the calculation of nuclear charge and current densities.

TABLE III. Total nuclear-polarization corrections (meV) to the $1s_{1/2}$, $2s_{1/2}$, $2p_{1/2}$, and $2p_{3/2}$ states of $^{208}_{82}Pb^{81+}$ in both the Feynman and Coulomb gauges. The abbreviation CNP denotes the unretarded results.

States	Present Feynman NP	Present Coulomb NP	Present CNP	Ref. [8] CNP
$1s_{1/2}$	−38.2	−37.0	−33.2	−29.3
$2s_{1/2}$	−6.7	−6.4	−5.7	−5.0
$2p_{1/2}$	−0.2	−0.2	−0.6	
$2p_{3/2}$	+0.0	+0.0	−0.0	

The results presented in the preceding section can be summarized as follows.

(1) In the Feynman (Coulomb) gauge, we obtained the NP energies of −38.2 (−37.0), −6.7 (−6.4), −0.2 (−0.2), and +0.0 (+0.0) meV for the $1s_{1/2}$, $2s_{1/2}$, $2p_{1/2}$, and $2p_{3/2}$ states, respectively.

(2) The transverse contribution is small in comparison with the CNP contribution. It is about 12% both for the $1s_{1/2}$ and $2s_{1/2}$ states. The present results confirm the estimates for the NP corrections presented earlier [8].

(3) The NP shifts of electronic atoms have serious gauge dependence if one calculates them with only the ladder and cross diagrams of the two-photon exchange processes. The NP energies for the $1s_{1/2}$ state due to these diagrams are +1.5 meV and −32.7 meV in the Feynman and Coulomb gauges, respectively. Inclusion of the seagull graph gives the NP energies of −38.2 meV and −37.0 meV. The seagull graph is quite important in restoring the gauge invariance of the NP calculation.

(4) We found that the nuclear dipole states have a predominant NP contribution. We also found that surprisingly large cancellations occur in the resulting NP energy. The ladder, cross, and seagull diagrams all give large contributions to the NP energy if their contributions from the positive- and negative-energy electron states are separately considered. Neglecting any one of these can introduce a non-negligible change in the NP energy, while inclusion of all these produces results very similar to the CNP calculations.

ACKNOWLEDGMENTS

We would like to thank N. Yamanaka and A. Ichimura for arousing our interest in the electronic-atom NP calculation.

APPENDIX: GAUGE INVARIANCE

To prove the gauge invariance of the NP energy, we write the sum of the ladder and cross contributions as follows:

$$\Delta E^L_{NP}+\Delta E^X_{NP}=-i\frac{(4\pi\alpha)^2}{2}\int\frac{d\omega}{2\pi}\int\frac{d\boldsymbol{q}}{(2\pi)^3}\int\frac{d\boldsymbol{q}'}{(2\pi)^3}\times\Pi^{\mu\nu}_e(\omega,\boldsymbol{q},\boldsymbol{q}')D_{\mu\xi}(\omega,\boldsymbol{q})D_{\zeta\nu}(\omega,\boldsymbol{q}')\times\Pi^{\xi\zeta}_N(\omega,\boldsymbol{q},\boldsymbol{q}'),\quad\text{(A1)}$$

where $\Pi_e^{\mu\nu}(\omega,\boldsymbol{q},\boldsymbol{q}')$ and $\Pi_N^{\xi\zeta}(\omega,\boldsymbol{q},\boldsymbol{q}')$ are the electronic- and nuclear-polarization tensors defined by

$$\Pi_e^{\mu\nu}(\omega,\boldsymbol{q},\boldsymbol{q}')=\sum_{i'}\left(\frac{j_e^{\mu}(-\boldsymbol{q})_{ii'}j_e^{\nu}(\boldsymbol{q}')_{i'i}}{\omega+\omega_e-iE_{i'}\epsilon}-\frac{j_e^{\nu}(\boldsymbol{q}')_{ii'}j_e^{\mu}(-\boldsymbol{q})_{i'i}}{\omega-\omega_e+iE_{i'}\epsilon}\right), \tag{A2}$$

$$\Pi_N^{\xi\zeta}(\omega,\boldsymbol{q},\boldsymbol{q}')=\sum_{I'}\left(\frac{J_N^{\xi}(\boldsymbol{q})_{II'}J_N^{\zeta}(-\boldsymbol{q}')_{I'I}}{\omega-\omega_N+i\epsilon}-\frac{J_N^{\zeta}(-\boldsymbol{q}')_{II'}J_N^{\xi}(\boldsymbol{q})_{I'I}}{\omega+\omega_N-i\epsilon}\right). \tag{A3}$$

Photon propagators in the Feynman and Coulomb gauges are related to each other by

$$D_{\mu\xi}^{C}(q,\omega)=D_{\mu\xi}^{F}(q,\omega)-\frac{1}{q^2+i\epsilon}\left(\frac{q_\mu q_\xi-\omega(q_\mu g_{\xi 0}+q_\xi g_{\mu 0})}{q^2}\right). \tag{A4}$$

If both $q_\mu\Pi_e^{\mu\nu}=0$ and $q_\xi\Pi_N^{\xi\zeta}=0$ are satisfied, it is easy to see that the Feynman and Coulomb gauges give the same result for the NP contributions given by Eq. (A1).

Multiplying both sides of the electronic-polarization tensor by q_μ, and using the continuity equation of the charge conservation, one obtains

$$\begin{aligned}q_\mu\Pi_e^{\mu\nu}(\omega,\boldsymbol{q},\boldsymbol{q}')&=\sum_{i'}\left[\langle i|\hat{\rho}_e(-\boldsymbol{q})|i'\rangle\langle i'|\hat{j}_e^{\nu}(\boldsymbol{q}')|i\rangle-\langle i|\hat{j}_e^{\nu}(\boldsymbol{q}')|i'\rangle\langle i'|\hat{\rho}_e(-\boldsymbol{q})|i\rangle\right]\\&=\langle i|[\hat{\rho}_e(-\boldsymbol{q}),\hat{j}_e^{\nu}(\boldsymbol{q}')]|i\rangle.\end{aligned} \tag{A5}$$

In deriving the second equality, we have assumed the completeness of the intermediate states of the electron. For the electromagnetic charge and current operators

$$\hat{\rho}_e(-\boldsymbol{q})=\begin{pmatrix}1&0\\0&1\end{pmatrix}e^{i\boldsymbol{q}\cdot\boldsymbol{r}},\quad \hat{j}_e(\boldsymbol{q}')=\begin{pmatrix}0&\boldsymbol{\sigma}\\\boldsymbol{\sigma}&0\end{pmatrix}e^{-i\boldsymbol{q}'\cdot\boldsymbol{r}} \tag{A6}$$

used with the Dirac-electron wave functions, the commutation relation in Eq. (A5) vanishes. Hence the gauge invariance $q_\mu\Pi_e^{\mu\nu}(\omega,\boldsymbol{q},\boldsymbol{q}')=0$ for the electronic-polarization tensor follows.

For the nuclear-polarization tensor, we can obtain a form similar to Eq. (A5) by assuming charge conservation as well as the completeness relation. In the present calculation, the impulse charge and current operators

$$\hat{\rho}_N(-\boldsymbol{q})=\sum_i^Z e^{i\boldsymbol{q}\cdot\boldsymbol{r}_i},$$

$$\hat{J}_N(\boldsymbol{q})=\sum_i^Z\frac{\vec{\boldsymbol{\nabla}}_{\boldsymbol{r}_i}-\overleftarrow{\boldsymbol{\nabla}}_{\boldsymbol{r}_i}}{2m_p i}e^{i\boldsymbol{q}\cdot\boldsymbol{r}_i}+\sum_i^A(\boldsymbol{\nabla}_{\boldsymbol{r}_i}\times\boldsymbol{\mu})e^{i\boldsymbol{q}\cdot\boldsymbol{r}_i} \tag{A7}$$

are employed with the nonrelativistic RPA calculation. The spin-current operator in the second term of $\hat{J}_N(q)$ commutes with $\hat{\rho}_N$. Hence the spin current introduces no gauge violation into the NP calculation of Eq. (A1). The convection current, on the other hand, does not commute with $\hat{\rho}_N$ leading to a violation of gauge invariance,

$$\langle I|[\hat{\rho}_N(-\boldsymbol{q}),\hat{j}_N^{\nu}(\boldsymbol{q}')]|I\rangle=\frac{\boldsymbol{q}}{m_p}\rho_N(\boldsymbol{q}-\boldsymbol{q}')_{II}. \tag{A8}$$

Therefore the NP contribution given by Eq. (A1) is not gauge invariant with the impulse charge-current operators. When the seagull tensor of Eq. (6) is added to the nuclear-polarization tensor of Eq. (A3), this term is just canceled. Hence the gauge invariance of NP calculation is restored by the seagull term together with the ladder and cross terms.

[1] H.F. Beyer, G. Menzel, D. Liesen, A. Gallus, F. Bosch, R. Deslattes, P. Indelicato, Th. Stöhlker, O. Klepper, R. Moshammer, F. Nolden, H. Eickhoff, B. Franzke, and M. Steck, Z. Phys. D: At., Mol. Clusters **35**, 169 (1995).

[2] J. R. Sapirstein and D. R. Yennie, in *Quantum Electrodynamics*, edited by T. Kinoshita (World Scientific, Singapore, 1990), p. 560.

[3] P.J. Mohr, G. Plunien, and G. Soff, Phys. Rep. **293**, 227 (1998).

[4] E. Borie and G.A. Rinker, Rev. Mod. Phys. **54**, 67 (1982).

[5] B. Hoffmann, G. Baur, and J. Speth, Z. Phys. A **315**, 57 (1984); **320**, 259 (1985).

[6] G. Plunien, B. Müller, W. Greiner, and G. Soff, Phys. Rev. A **39**, 5428 (1989); **43**, 5853 (1991).

[7] G. Plunien and G. Soff, Phys. Rev. A **51**, 1119 (1995); **53**, 4614(E) (1996).

[8] A.V. Nefiodov, L.N. Labzowsky, G. Plunien, and G. Soff, Phys. Lett. A **222**, 227 (1996).

[9] R.K. Cole, Jr., Phys. Rev. **177**, 164 (1969).

[10] Y. Tanaka and Y. Horikawa, Nucl. Phys. A **580**, 291 (1994).

[11] N. Yamanaka and A. Ichimura, Phys. Scr., T **T80**, 488 (1999).

[12] N. Yamanaka, Y. Horikawa, and A. Ichimura, Hyperfine Interact. **127**, 297 (2000).

[13] N. Yamanaka, A. Haga, Y. Horikawa, and A. Ichimura, Phys. Rev. A **63**, 062502 (2001).

[14] J.L. Friar and M. Rosen, Ann. Phys. (N.Y.) **87**, 289 (1974).

[15] R. Rosenfelder, Nucl. Phys. A **393**, 301 (1983).

[16] G.A. Rinker and J. Speth, Nucl. Phys. A **306**, 360 (1978).

[17] A.B. Migdal, *Theory of Finite Fermi Systems and Applications to Atomic Nuclei* (Interscience, New York, 1967).

[18] A. Bohr and B.R. Mottelson, *Nuclear Structure* (Benjamin, New York, 1975), Vol. 2, p. 399.

[19] Y. Horikawa and Y. Tanaka, Phys. Lett. B **409**, 1 (1997).